Supporting Information:

Surface Ligand Promotion of Carbon Dioxide Reduction through Stabilizing Chemisorbed Reactive Intermediates

Zhijiang Wang, [†,‡,*] Lina Wu, [⊥] Kun Sun, [†] Ting Chen, [‖] Zhaohua Jiang, [†,‡] Tao Cheng, [§,*] and William A. Goddard III [§,*]

[†] State Key Laboratory of Urban Water Resource and Environment, and [‡] School of Chemistry and Chemical Engineering, Harbin Institute of Technology, Harbin 150001, China;

[⊥]Molecular Imaging Research Center of Harbin Medical University, the Fourth Hospital of Harbin Medical University, Harbin 150001, China;

[‖] University of Oxford, Department of Chemistry, South Parks Road, Oxford OX1 3QR, United Kingdom;

[§]Materials and Process Simulation Center (MSC) and Joint Center for Artificial Photosynthesis (JCAP), California Institute of Technology, Pasadena, California 91125, United States.

*Correspondence to wangzhijiang@hit.edu.cn, tcheng@caltech.com, wag@wag.caltech.edu.

Materials and Methods

Materials

All the chemicals, including silver nitrate, cysteamine, 11-Amino-1-undecanethiol (AUT), ethylene glycol (EG), were obtained from Sigma-Aldrich and utilized as received. Ag foil (99.998% metal basis) was purchased from Alfa Aesar. carbon black was obtained from Cabot Corporation. Ultrapure water was from a Millipore Autopure system.

Synthesis of Ag NPs

C_2-Ag NPs: The cysteamine-functionalized silver NPs deposited on carbon black were prepared by the one-pot wet chemical approach. Before the reaction, carbon black was first sintered at 180 ºC for 10 h purged with Ar and then followed purged with 1000 ppm H_2S for 1 h. The molar ratio for Ag:cysteamine being 2:1. initially, carbon black (1.667 mmol) and cysteamine (0.059 mmol) were added into a 10 mL EG solution in an ultrasonic bath to obtain a well dispersed suspension. Then, this suspension was added to silver precursor solution which was $AgNO_3$ (0.118 mmol, the ratio of Ag ion to NH_2 being 2:1) dissolved in 10 mL of EG solution and kept at 50 °C for 0.5 h. The silver salt solution was subsequently heated to 160 °C at a rate of 3 °C min^{-1} and holding for 3 h. After cooling to room temperature, the products were washed with ethyl acetate several times and dried in a vacuum oven.

Ligand-free Ag NPs: The carbon black supported naked Ag NP were synthesized in two steps. Firstly, the Ag NPs were prepared by chemical reduction method. Secondly, the Ag NPs were loaded on carbon blacks and removed the ligands. Aqueous solutions containing $NaBH_4$ (2.0×10^{-3} mol L^{-1}) and sodium citrate (4.5×10^{-3} mol L^{-1}) were heated to 60 ºC and kept for 0.5 h in the dark with vigorous stirring. $AgNO_3$ (1.0×10^{-3} mol L^{-1}) was then added drop-wise. The temperature of the solution was increased to 90 ºC. Subsequently, the pH value of the solution was adjusted to 10.5 using 0.1 M NaOH while keeping further heated for 20 minutes. After cooled to room temperature, the NP suspension was washed thrice. Followed, the prepared Ag NPs were deposited onto the carbon black by sonicating the mixture of Ag NPs dispersion and carbon black. The solvent was decanted and the precipitate was washed. The dried powder was annealed overnight at 180 ºC in vacuum to remove the surfactant.

C_{11}-Ag NPs: These Ag NPs were prepared with the method similar with C_2-Ag NPs except changing the surface ligands.

Ag foil modified by cysteamine: Ag foil electrodes were modified through immersing one polished Ag foil into ~10 mL of water solution which contained 5×10^{-6} mmol cysteamine. The solution was bubbled with N_2 for 1 h in advance.

Characterizations

XRD patterns of the samples were recorded on a Bruker AXS D5000 diffractometer. TEM images were obtained on a Tecnai G2 F30 electron microscope under an accelerating voltage of 300 keV. TEM samples were prepared by dropping a diluted suspension onto amorphous carbon-coated copper grids and drying in the air.

XPS of samples was measured using a PHI 5700 X-ray photoelectron spectrometer equipped with a monochromatic Al Kα X-ray source. ATR-IR spectra of the samples were monitored by an Agilent Cary 600 Series FTIR spectrometer, equipped with a multiple-reflection ATR accessory (PIKE Technologies, custom-modified GladiATR). The IR beam was detected by narrow-band mercury cadmium telluride detector cooled to 77 K. The spectra were collected on the Ge ATR crystal. The background was subtracted and a baseline correction was proceeded to eliminate minor fluctuations.

Preparation of working electrode

To prepare the different ligand-capped Ag NP on pyrolytic graphite edge-plane (PGE) electrodes, 5 mg Ag NPs were mixed with 950 μL isopropanol and 50 μL 5 wt% Nafion solution by sonication for 0.5 h to form a homogeneous ink. Subsequently, 5 μL suspension was drop-dried onto a PGE electrode.

Electrochemical Measurements

All electrochemical experiments were performed in a three-electrode system using an Autolab Potentiostat. The airtight two-compartment electrochemical cell was separated by an anion exchange membrane with 0.5 M $NaHCO_3$ electrolyte (pH 7.2) in each chamber. The electrolyte in the cathodic compartment was stirred magnetically at a rate of 1000 rpm during electrolysis. A piece of platinum wire was used as the counter electrode. All potentials were measured against an Ag/AgCl reference electrode (3.0 M KCl) and converted to the reversible hydrogen electrode (RHE) reference scale using

$$\text{E (vs RHE)} = \text{E (vs Ag/AgCl)} + 0.210 + 0.0591 \times \text{pH} \quad \text{(S1)}$$

Before electrolysis, the electrolyte in the cathodic compartment was bubbled with CO_2 gas for 1 h. A steady supply of CO_2 gas was delivered at a rate of 5.0 sccm. The cathode compartment was vented directly into the sampling loop of a gas chromatograph (GC, Aglient 7890A). The GC analysis was set up to split the gas sample into two aliquots. One aliquot passed a thermal conductivity detector (TCD), and the other was routed through flame ionization detector (FID). ^{1}H NMR was employed to test for possible liquid-phase products. Their concentration was analyzed on Bruker Avance 400 MHz spectrometer. All potentials were *iR*-corrected. The corrected method is in accordance with previous report [1].

The electrochemical surface area of the working electrode was determined by lead (Pb) underpotential deposition (UPD) in solution containing 1 mM $Pb(acetate)_2$, 1 mM $HClO_4$ and 0.5 M $NaClO_4$. Scan rate is 10 mV s^{-1}. Pb UPD desorption peak from -0.32 to -0.17 V was integrated to calculate the electrochemical surface area, assuming 420 μC cm_{ec}^{-2} for all the Ag-based electrodes.

Turnover frequency (TOF) for CO production on the various electrodes is calculated by using following equation.[2] The number of active Ag centers is determined by Pb UPD experiment.

$$TOF = \frac{Volumetric\ rate\ of\ reaction}{number\ of\ active\ centers} \quad \text{(S2)}$$

The Faradaic efficiency and partial current of H_2 and CO production ($FE_{H2\ or\ CO}$ and $i_{H2\ or\ CO}$) were calculated from GC chromatogram peak areas where $V_{H2\ or\ CO}$ is volume concentration of H_2 or CO based on the calibration of the GC. The equation is as following.

$$i_{H_2 or\ CO} = V_{H_2\ or\ CO} \times Q \times \frac{2Fp_0}{RT} \quad \text{(S3)}$$

$$FE_{H_2 or\ CO} = \frac{i_{H_2\ or\ CO}}{i_{total}} \times 100 \quad \text{(S4)}$$

Where i_{total} is measured current, F is Faradaic constant, p_0 is pressure, T is temperature and R is ideal gas constant, 8.314 J mol K^{-1}.

Computational details

To simulate the water/Ag (111) interface we used 32 explicit water molecules (5 layers, 11.77 Å thick) on a 3×3 Ag (111) surface slab (4 layers) with an area of 67.64 $Å^2$. The simulation box was extended to 40 Å along the z axis with a vacuum of 24 Å.

Electronic structure calculations were performed within the DFT framework, as implemented in the Vienna ab initio simulation program (VASP), [3-5] a plane-wave pseudopotential package. The exchange and correlation energies were calculated using the Perdew, Burke, and Ernzerhof (PBE) functional within the generalized gradient approximation (GGA).[6] The projector augmented wave (PAW) method[7] was used to account for core-

valence interactions. We used a plane-wave cutoff energy of 400 eV and the First order Methfessel-Paxton scheme with a smearing width of 0.2 eV. Dipole corrections were applied along the z axis. The PBE-D3 method was used to include London dispersion.

We used a 1.2 fs time step in the Molecular Dynamics (MD) simulations with the hydrogen mass set to 2 amu. These MD simulations used only the gamma point of the Brillouin zone with no consideration of symmetry. The velocities were rescaled every 20 MD steps to readjust the target temperature to equilibrium. We employed a Nose Hoover thermostat for the free energy calculations with a temperature damping parameter of 100 fs.

Starting from this well-equilibrated interface, we carried out 10 ps of ab initio AIMD simulation at 298 K. After that, we used metadynamics and thermodynamic integration to generate the reactive trajectories using the following parameters: the height of Gaussian hill (h) is 0.08 eV; the width of Gaussian hill (w) is 0.18 Å; the updating frequency is 24 fs. We applied a Gaussian wall at z = 5.0 Å to prevent CO_2 escaping from the surface (the opposite direction). Thus, approaching to the surface is the only allow direction. Thermodynamics integration was further employed to converge the free energy results with 11 windows by using constraint molecule dynamics.

Supporting Figures

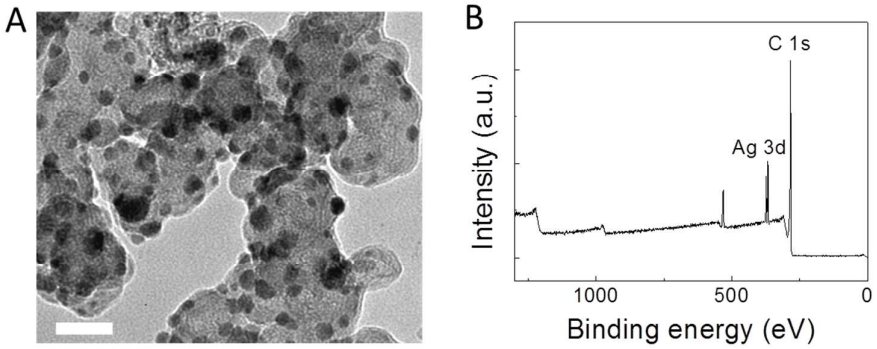

Figure S1. Characterization of naked Ag NPs**.** (a) TEM image (scale bar, 40 nm); (b) XPS spectrum. TEM image shows that naked Ag NPs are loaded onto carbon blacks and have particle sizes of around 10 nm.

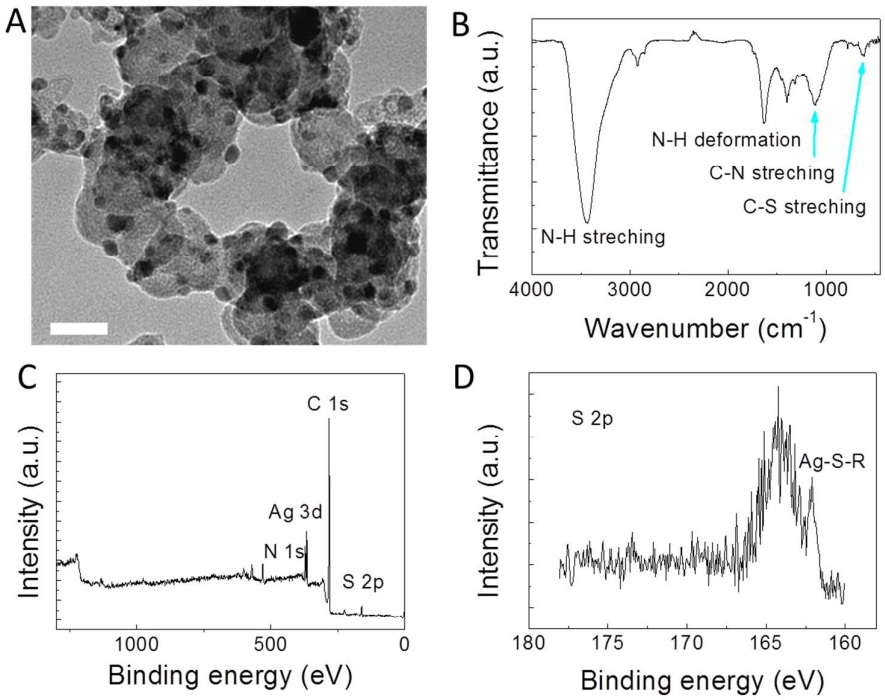

Figure S2. Characterization of C_{11}-Ag NPs. (a) TEM image (scale bar, 40 nm); (b) FT-IR spectrum; (c) XPS spectrum; and (d) high resolution S 2*p* XPS spectrum. TEM image shows that C_{11}-Ag NPs are loaded onto carbon blacks and have particle sizes of around 10 nm. FT-IR spectrum indicates the presence of AUT molecules on Ag NPs. XPS spectra confirm the assembly of AUT on Ag by Ag-S bonding.

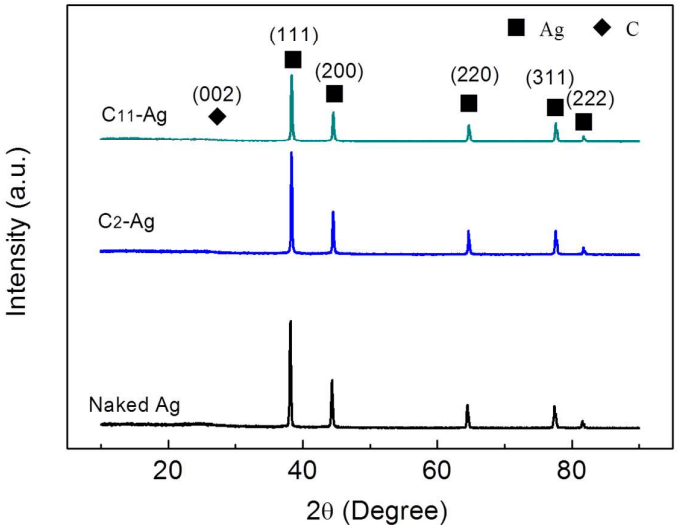

Figure S3. XRD patterns of different ligand-capped Ag NPs.

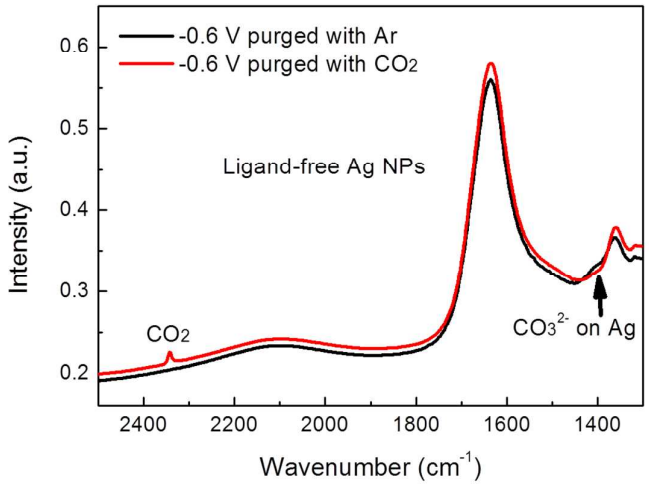

Figure S4. *In situ* ATR-IR spectra of ligand-free Ag NPs at -0.6 V purged with Ar or CO_2. The electrolyte is 0.1 M $NaHCO_3$ resolved in H_2O.

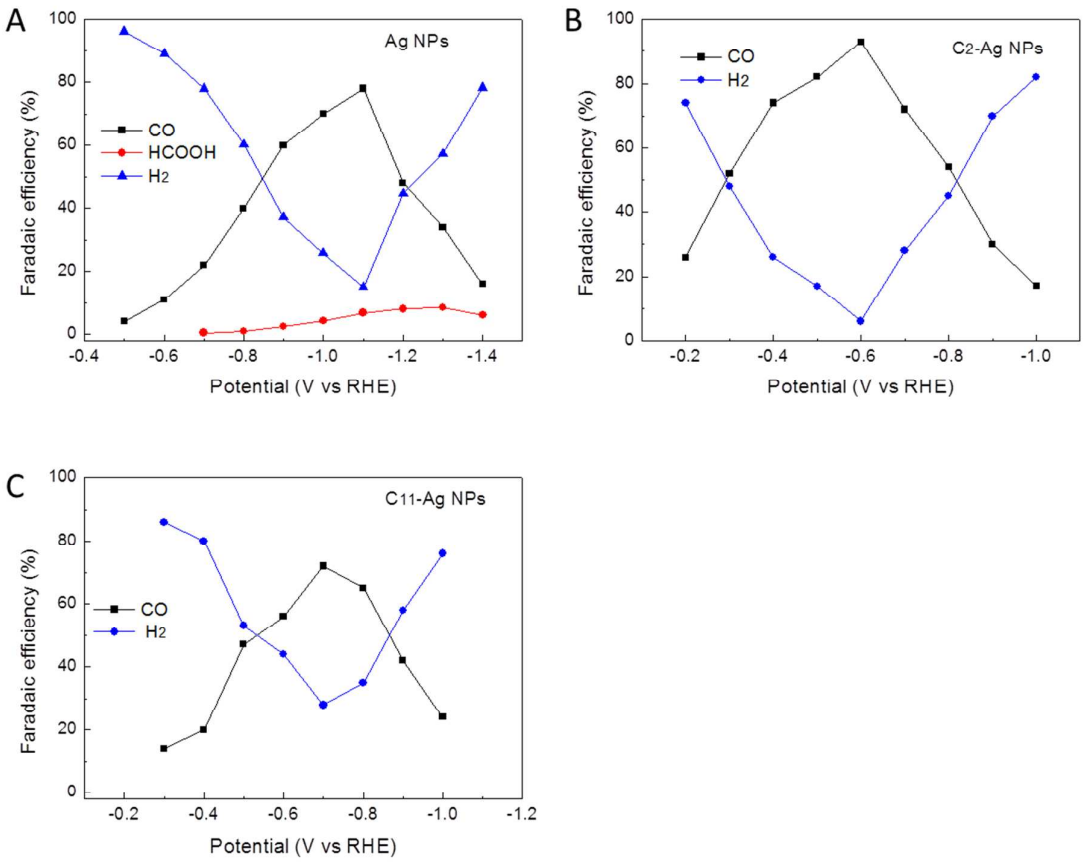

Figure S5. FE for each product as a function of potential on different Ag NP electrodes**.** (a) ligand-free Ag NPs; (b) C_2-Ag NPs; and (c) C_{11}-Ag NPs.

The CO_2 reduction activity of C_2-Ag NPs shows a dependence on the molar ratio of cysteamine (CA) to $AgNO_3$. Figure S7 presents the catalytic activity of four C_2-Ag NCs synthesized under the $AgNO_3$:CA molar ratio as 10:1, 5:1, 2:1 and 1:10. Both the selectivity and activity of C_2-Ag NCs exhibit a volcanic-type relationship with the amount of CA. When the $AgNO_3$:CA ratio is 2:1, the Ag NPs present the best catalytic property. The further increasing or decreasing CA amount degrades the catalytic activity. The activity has a requirement on the CA in a moderate amount.

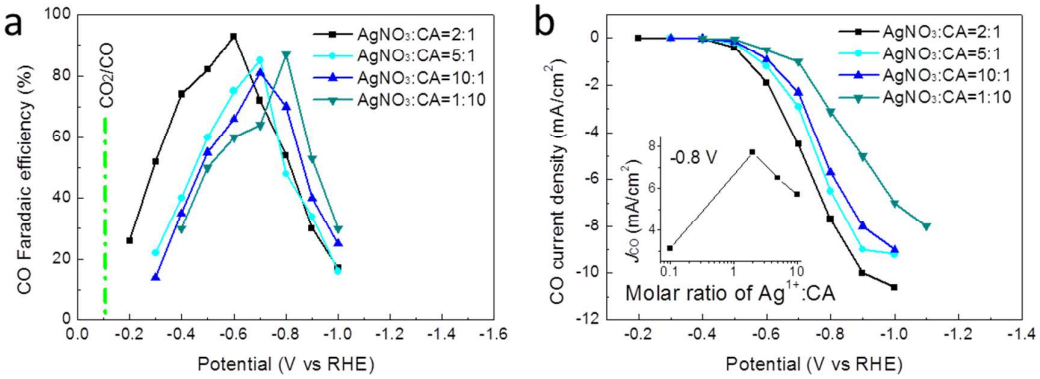

Figure S6. Influence of molar ratio of $AgNO_3$:CA on the catalysis. (a) FE for CO vs potential. (b) CO partial current density vs potential. The inset in figure b shows the CO partial current density at -0.8 V vs molar ratio of $AgNO_3$:CA.

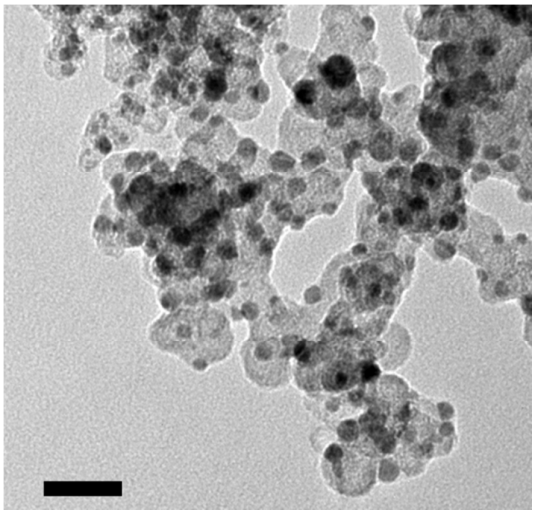

Figure S7. TEM image of C_2-Ag NPs after electrolysis lasted for 10 h. Scale bar is 40 nm. There is no big difference on morphology compared to pristine C_2-Ag NPs.

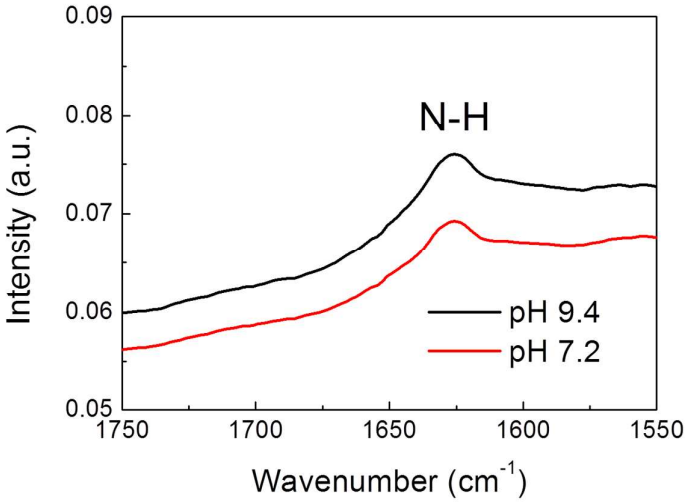

Figure S8. *In situ* ATR-IR spectra of C_2-Ag in $NaHCO_3$ solution with pH value being 9.4 and 7.2.

As shown in Figure S8, the vibrational frequencies of plane deformation of the NH are almost the same at pH = 7.2 and 9.4. Thus, it seems that pH has little influence on the plane deformation of the NH. Therefore, the small red shift observed under electro-reduction condition is possibly associated with the appearance of reactive intermediate, in which case chemisorbed CO_2 is the most possible candidate.

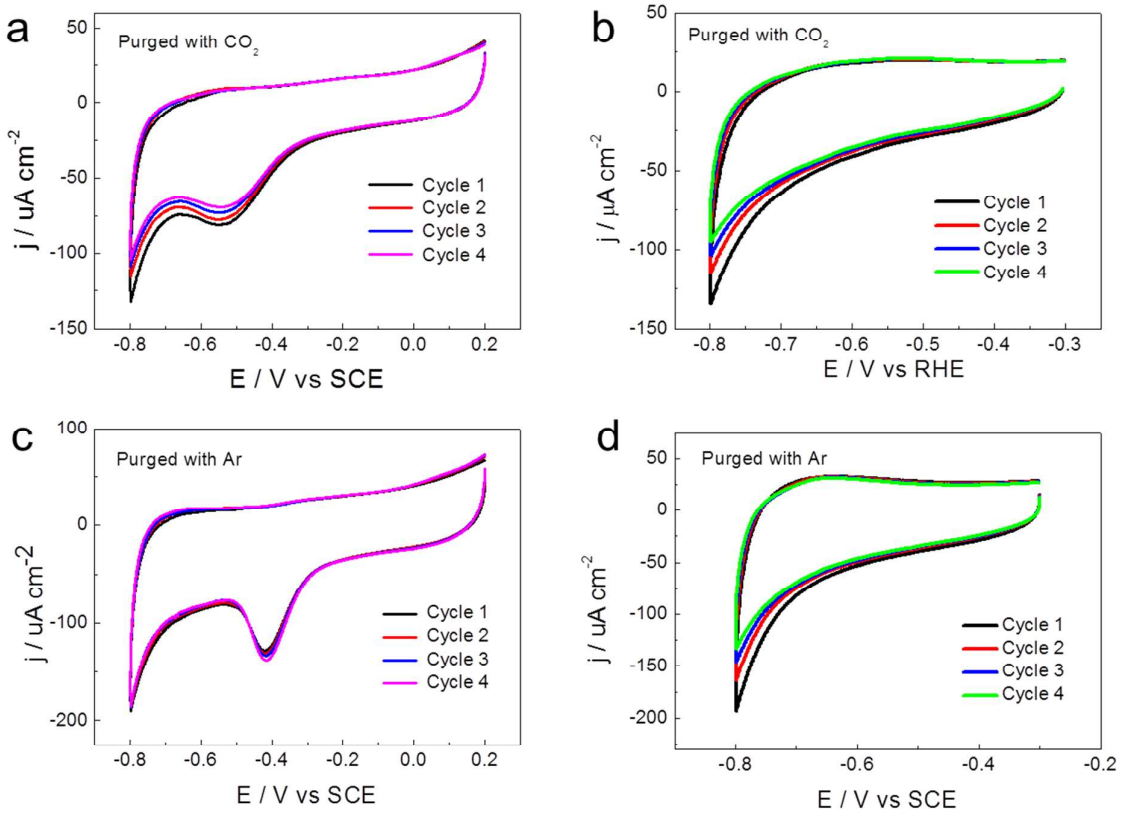

Figure S9. Cyclic voltammograms for cysteamine-capped Ag NPs with four consecutive scans in 0.5 M $NaHCO_3$ solution saturated by CO_2 in potential windows of (+0.2 V ~ -0.8 V) (a) and (-0.3 V ~ -0.8 V) (b), and purged with Ar in potential windows of (+0.2 V ~ -0.8 V) (c) and (-0.3 V ~ -0.8 V) (d). The sweep rate is 0.01 V/s.

Basing on Figure S9, it can be found that the cysteamine-capped Ag NPs keep very high stability. The peak at around -0.5 V vs SCE is caused by cleavage of Ag-S bonds. In absence of CO_2 in the electrolyte, this peak locates at -0.42 vs SCE. When the electrolyte is purged with CO_2, this peak is shifted to -0.54 vs SCE. This shift is caused by the variation of pH value. If the alkanethiol ligands have poor stability, the Ag-S peak in cyclic voltammogram curves will disappear at the second cathodic scans. For the synthesized cysteamine-capped Ag nanoparticles, the peaks corresponding to Ag-S show a little variation under four consecutive scans. When the CV cycling potential range is in -0.8 to -0.3 V, the oxidation of Ag-S is depressed. There is no Ag-S reduction peak any more. But if the scan potential is extended to -0.8 to 0.2 V, this peak at around -0.5 V will appear again. This gives a strong evidence that the stability of the cysteamine on Ag NPs under electrochemical conditions can keep very well both in the presence and absence of CO_2.

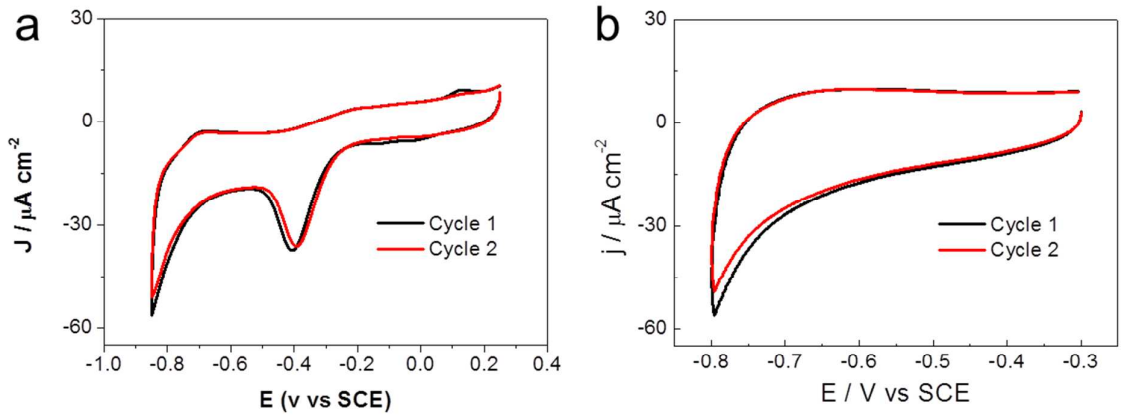

Figure S10. cyclic voltammograms (CV) of C_{11}-Ag NPs with two consecutive scans in 0.5 M $NaHCO_3$ solution saturated by CO_2 in potential windows of (+0.2 V ~ -0.8 V) (a) and (-0.3 V ~ -0.8 V) (b) with a sweep rate of 0.01 V/s.

The C_{11} ligand has a good stability on Ag NP. As reported in previous research, if the alkanethiol ligands has a poor stability on noble metals, the Ag-S peak in cyclic voltammogram curves will disappear at the second cathodic scan. Figure S10a shows the cyclic voltammograms of C_{11}-Ag NPs in potential windows of +0.2 V ~ -0.8 V. The peak at -0.36 vs SCE is corresponding to cleavage of the Ag-S bond. It can be found at the second cathodic scan, there is a little shift on the CV curve. This peak still keeps very clear. When the CV potential windows in decreased to -0.3 V ~ -0.8 V (Figure S10b), the oxidation of Ag-S is depressed. There is no Ag-S reduction peak any more. But if the scan potential is extended to -0.8 to 0.2 V, this peak at around -0.36 V will appear again. So, the C_{11} ligand has a good stability on Ag NP.

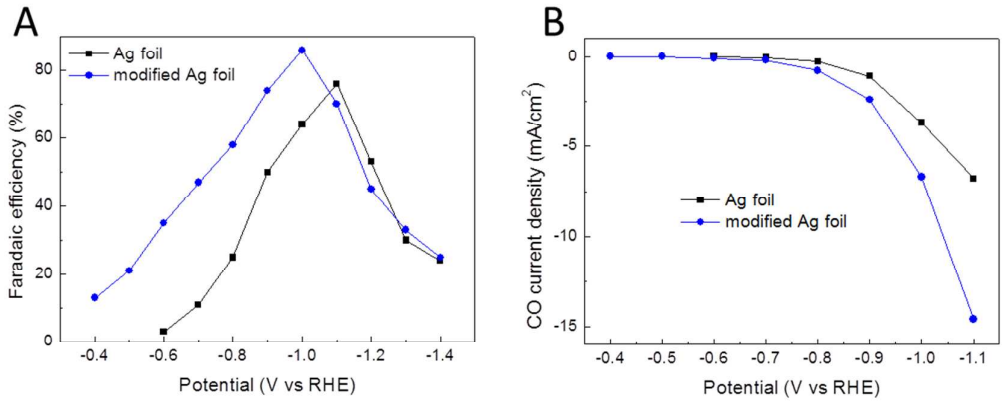

Figure S11. Electrocatalytic performance of Ag foil before and after modified with cysteamine. (a) FE for CO vs potential; (b) CO partial current density vs potential.

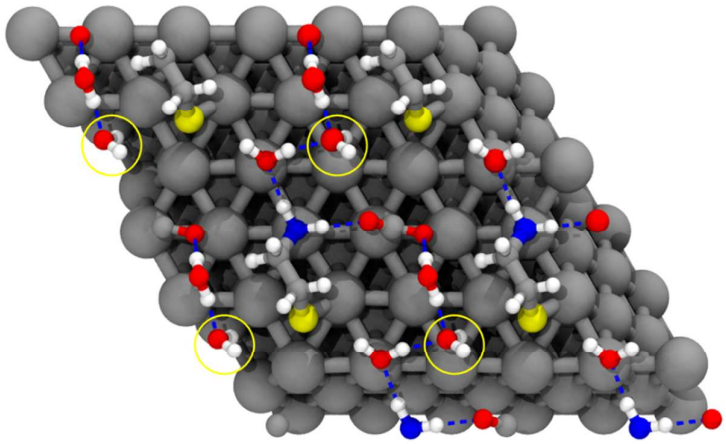

Figure S12. The optimized geometry from HSE06 functional from a 2×2 supercell. The colors are Ag in silver, C in gray, S in yellow, N in blue and H in white. The hydrogen-bonds are shown in dashed blue. The highlighted (yellow circled) water molecule is fixed in the optimization, because it has a dangling hydrogen bond, which interacts with the second layer of water in explicit solvent calculation.

we carried out the geometry optimization by taking the snapshot from PBE AIMD simulations. In HSE calculation, we only keep cysteamine, chemisorbed CO_2 and water molecules that directly involved in the hydrogen bond network with chemisorbed CO_2. The HSE parameters are specified for HSE06, which are 0.25 of the mixing parameter and 0.2 of the adjustable parameter controlling the short-rangeness of the interaction.

The optimized geometry is show in Figure S14, which shows two hydrogen bonds stabilize the chemisorbed CO_2: one from N-H (cysteamine) and one from O-H (water). This is similar as we observed in our PBE AIMD simulation. Thus, we conclude that the PBE level of calculation can well reproduce the geometry, which is confirmed from more expensive hybrid calculation.

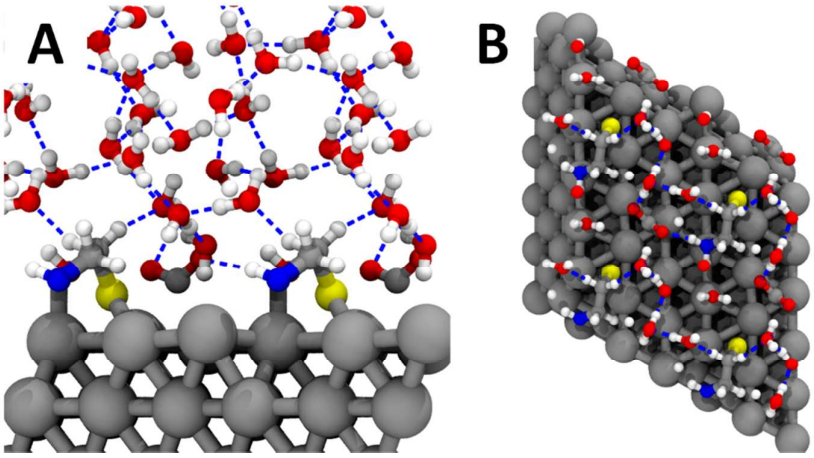

Figure S13. The snapshot from PBE AIMD simulation shows the geometry of chemisorbed CO_2 in replicated 2×2 supercell from side view (A) and top view (B). The isolated hydrogen and dangling bonds are due to artificial effect in plotting periodic structures and cutting for the first layer of water for viewing convenience.

We employed a 3×3 Ag (111) with one cysteamine leading to a surface concentration of 1/9 ML, which is closest to the experiment condition. We added one figure showing a 2×2 supper cell of our simulation box, which demonstrates that cysteamine is far from its periodic boundary condition (PBC) image and CO_2 is also far from its PBC images as show in Figure S12 from side view (Figure S13A) and top view (Figure S13B). Thus, we consider 3×3 model is large enough to accommodate 1/9 ML cysteamine and 1/9 ML CO_2 without apparent PBC artificial effect.

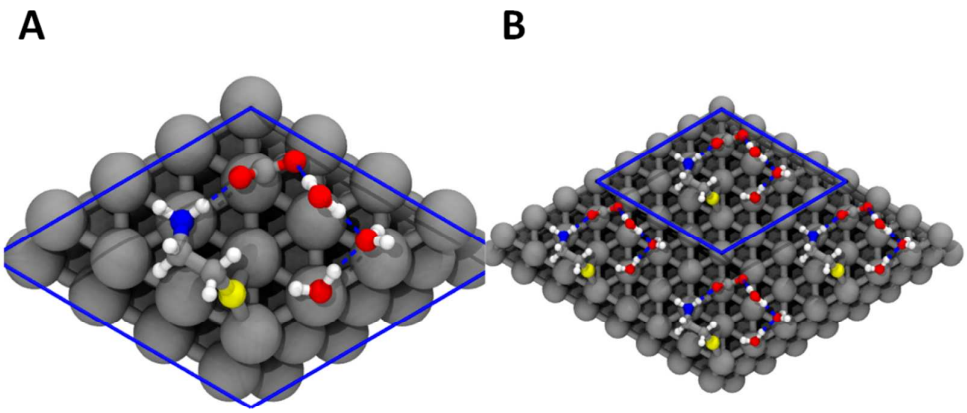

Figure S14. The optimized geometry on a 4×4 Ag(111) surface. (A) unit cell and (B) replicated 2×2 supercell.

Increasing the cell size can further reduce the chance of lateral interaction, although it also dilutes the surface concentration to 1/16 ML, lower than the experiment condition. As shown in Figure S14, we also observed similar hydrogen bond network as that in 3×3.

Supporting Table

Table S1. Comparison of CO_2 reduction activity for C_2-Ag NPs electrocatalysis with other reported Ag catalysts. Mass activity is not reported by Ref R8. The Ag nano-corals were prepared on Ag foil. According to the surface feature and reduction activity, their mass activity is comparable to that of nanoporous Ag reported in R6, but far lower than the value of C_2-Ag NPs.

Ref	Catalysts	Ag loading amount (mg/cm^2)	Applied potential (V)	J_{CO} (mA/cm^2)	Mass activity (mA/mg)
This work	C_2-Ag NPs	0.08	0.5	0.4	4.01
Ref[8]	Nanoporous Ag	~40	0.5	8	0.20
Ref[8]	Ag NPs	1.0	0.5	0.022	0.022
Ref[9]	Ag NPs	0.09	0.5	0.23	2.56
Ref[2]	Ag nano-corals	>40	0.5	1.1	N/A[a]

References

(1) Kuhl, K. P.; Cave, E. R.; Abram, D. N.; Jaramillo, T. F. New Insights into the Electrochemical Reduction of Carbon Dioxide on Metallic Copper Surfaces. *Energy Environ. Sci.* **2012,** *5*, 7050-7059.

(2) Hsieh, Y.-C.; Senanayake, S. D.; Zhang, Y.; Xu, W.; Polyansky, D. E. Effect of Chloride Anions on the Synthesis and Enhanced Catalytic Activity of Silver Nanocoral Electrodes for CO2 Electroreduction. *ACS Catal.* **2015,** *5*, 5349-5356.

(3) Kresse, G.; Hafner, J. Ab Initio Molecular Dynamics for Liquid Metals. *Phys. Rev. B: Condens. Matter Mater. Phys.* **1993,** *47*, 558-561.

(4) Kresse, G.; Furthmüller, J. Efficiency of Ab-initio Total Energy Calculations for Metals and Semiconductors Using a Plane-wave Basis Set. *Comput. Mater. Sci.* **1996,** *6*, 15-50.

(5) Kresse, G.; Furthmüller, J. Efficient Iterative Schemes for Ab Initio Total-energy Calculations Using a Plane-wave Basis Set. *Phys. Rev. B: Condens. Matter Mater. Phys.* **1996,** *54*, 11169-11186.

(6) Perdew, J. P.; Burke, K.; Ernzerhof, M. Generalized Gradient Approximation Made Simple. *Phys. Rev. Lett.* **1996,** *77*, 3865-3868.

(7) Kresse, G.; Joubert, D. From ultrasoft pseudopotentials to the projector augmented-wave method. *Phys. Rev. B: Condens. Matter Mater. Phys.* **1999,** *59*, 1758-1775.

(8) Lu, Q.; Rosen, J.; Zhou, Y.; Hutchings, G. S.; Kimmel, Y. C.; Chen, J. G.; Jiao, F. A Selective and Efficient Electrocatalyst for Carbon Dioxide Reduction. *Nat. Commun.* **2014,** *5*, 3242.

(9) Kim, C.; Jeon, H. S.; Eom, T.; Jee, M. S.; Kim, H.; Friend, C. M.; Min, B. K.; Hwang, Y. J. Achieving Selective and Efficient Electrocatalytic Activity for CO_2 Reduction Using Immobilized Silver Nanoparticles. *J. Am. Chem. Soc.* **2015,** *137*, 13844-13850.